Modeling and Implementation of an Open-loop Single-axis Solar Tracking System Driven by an SMA Spring Actuator

Saja M. Abbas
Electromechanical of Electromechanical Engineering, University of Technology

Jamal A.-K. Mohammed
Electromechanical of Electromechanical Engineering, University of Technology

Wisam E. Abdul-Lateef
Electromechanical of Electromechanical Engineering, University of Technology

https://doi.org/10.5109/7326949

出版情報：Evergreen. 11 (4), pp.3109-3118, 2024-12. Interdisciplinary Graduate School of Engineering Sciences, Kyushu University, Japan
バージョン：

Modeling and Implementation of an Open-loop Single-axis Solar Tracking System Driven by an SMA Spring Actuator

Saja M. Abbas*, Jamal A.-K. Mohammed, Wisam E. Abdul-Lateef
Electromechanical of Electromechanical Engineering, University of Technology, Baghdad, Iraq

*Author to whom correspondence should be addressed:
E-mail: eme.22.24@grad.uotechnology.edu.iq

(Received August 9, 2024; Revised October 22, 2024; Accepted November 3, 2024).

Abstract. Solar panels must maintain the vertical direction of sunlight throughout the day to optimize their electrical energy output. Different actuators, such as electric, hydraulic, or pneumatic, can accomplish the tracking mechanism. However, there are several issues with these actuators, including their affordability, size, complexity of their control circuits, and maintenance requirements. Smart materials called shape memory alloys (SMAs) have replaced traditional actuators to address these issues. The SMA has special qualities that make it crucial in designing a solar panel sun-tracking system. When heated or subjected to a direct electric current, the SMA spring may function as a linear actuator, contracting with significant force. On the day the test is being conducted, the current data might be kept in an Excel sheet table according to the sun's azimuth angles. This study aims to model by Matlab/Simulink and implement an SMA actuator (spring) driven single-axis solar tracker in the azimuth direction under open-loop control. The results show that, in comparison to the fixed panel, the mobile solar panel's maximum efficiency will increase by 30% at noontime solar radiation values of 1026 W/m^2. Additionally, these alloys help to raise the average efficiency of the moving plate's increase by 60% when compared to the stationary panel. To validate the computational model results, experimental tests have been conducted on an SMA-based solar tracker setup. The simulated and experimental results appear to correlate well. The results also indicate that this alloy is a good actuator for driving solar trackers.

Keywords: Solar tracking system; SMA actuator; excitation current; PV panel; Azimuth angle

1. Introduction

Renewable energy sources[1], such as solar, wind, and other sources, are gaining popularity among users as an alternative to fossil fuels. Solar energy is one of the most attractive and healthy alternatives to fossil fuels. Solar energy has several uses, such as crop drying systems[2–4], air heating systems[5,6], water heating systems[7,8], and the production of electricity[9,10], etc. Because clean energy is becoming increasingly important, there is a greater demand for solar energy equipment. Hydro, wind, solar, and environmental energy[9] are some of the methods utilized to supply the growing need for electrical energy and accomplish sustainability goals.

Solar-powered equipment is widely used in residential, commercial, and agricultural settings. Solar panels are by far the most common component of this kind of equipment. To capture as much solar energy as feasible, these panels need to be combined with solar tracking systems[11] so that sunlight always falls perpendicular to the panels. Actuators must be installed in the tracking systems to implement the tracking mechanism.

Because actuators are essential to solar tracking systems, their design must be properly thought out. Strong durability capabilities, technical precision and control, stability, and seamless integration with solar trackers are all requirements for actuators. Good tracking of solar energy using actuators may increase the efficiency of solar panels by 30-40% compared to fixed panels[11].

Energy sources such as hydraulic pressure, pneumatic pressure, or electrical current may drive actuators. They convert energy into movement. It allows photovoltaic (PV) panel angle adjustments by users. According to degrees of structural freedom, solar tracking systems may be divided into two primary categories: single-axis[12,13] and dual-axis[14,15]. Single-axis trackers typically go in the direction of the sun, from east to west (the azimuth angle), while dual-axis trackers are designed to monitor the sun using two axes that correspond to the azimuth and altitude solar angles. Because single-axis tracking systems are easier to install and operate, have a longer lifespan, are more dependable, and are less expensive than dual-axis trackers, they are widely utilized in a wide range of applications. To achieve high structural dependability and control accuracy for the real performance of these systems, new designs and technologies for actuators in both kinds of trackers have been developed recently.

Mechanical actuators come in various forms, including stepper motors[16], DC motors and gearboxes[17], and linear motors[18]. The solar tracker can also be driven by different actuators, such as pneumatic[19] and hydraulic[20].

To increase the efficiency of solar panels, particularly in hot regions, Mohammed et al.[14] developed and experimentally verified the efficiency of a PV panel integrated with a water glazing system and driven by a dual-axis solar tracker. Hamidi et al.[15] developed and built an automated dual-axis sun tracker driven by two worm DC gear motors and controlled by a microcontroller to deliberately point the solar concentrator prototype in the direction of the sun in order to improve its thermal performance. Khalaf et al.[21] designed and constructed, by Matlab/Simulink, a model of fuzzy logic-controlled, closed-loop, dual-axis solar tracker powered by pneumatic actuators. Abdul-Hussein et al.[22] designed suitable pneumatic actuators to drive an open-loop, two-axis PV solar tracker while taking into consideration the maximum load and impact angles in the worst weather conditions experienced in Iraq. Alexandru[20] created a simulation model of a dual-axis solar tracker that is hydraulically operated and utilized in a PV platform. Hydraulic linear actuators were used to drive the PV panel.

The use of electrical actuators in driving the solar tracker makes it work well, but it suffers from many defects, including their large size and weight, the economic cost of the actuators, the electrical losses associated with their operation, as well as the complexity and cost of their control circuits. As for the hydraulic and pneumatic systems, they are highly adaptable and can be used in a wide range of applications, including solar trackers, they are frequently subject to fluid leaks and require additional components (compressors, pumps, valves, and piping). Numerous drawbacks are common to these actuators, such as the necessity for extra parts, lengthy installation times, high system complexity, hefty weight, and high power consumption. Smart alloys known as shape memory alloys (SMAs) were used to replace these actuators to address these issues.

The SMA actuator, a smart material, has several qualities, including compactness, robustness, high strength-to-weight ratio, cheap cost, noiseless operation, and tiny size[23-25]. Due to its unique mechanical and thermal characteristics, it may be used in a wide range of technical applications. The material's shape memory effect allows it to return to its original form when the right stimulus is present[27]. The SMA can convert electrical energy into mechanical energy (motion). This task is usually completed by an electrical motor, yet in a few situations, the SMA provides notable benefits over motors[26].

Because of their enormous and attractive features, SMAs have become the focus of researchers' attention to study their unique properties and employ them in many applications. The SMAs have been the subject of recent studies in the fields of robotics[27], biomedicine[28], automotive[29], aerospace[30], and antennas[31].

Since these alloys have all the above-mentioned features and are used efficiently in many applications, the current study is distinguished from other studies by applying these smart and inexpensive alloys in implementing a solar tracking device. The present paper aims to model using Matlab Simulink and implement a smart single-axis sun tracker setup using the SMA mechanism under open-loop control. Using SMA actuators, this mechanism allows the PV panel to track the sun with an azimuth angle of 216° from sunrise at 5:09 to sunset at 18:49 during the day. By injecting a DC electric current into the SMA springs mounted on the tracker structure, these springs generate enough force to guide the solar PV panel to precisely track the sun's movement throughout the day. Sun tracking systems work better when they use SMA spring-based actuators because they provide smooth and accurate control, easy integration into the system architecture, and the possibility of downsizing, all while maintaining exceptional functional performance conditions.

An SMA-based solar tracking system setup was used to study the performance of the system as well as to experimentally test and confirm the accuracy of the computational model results.

2. Working principle of shape memory alloy

The material's phase transition behavior gives the SMA its thermo-mechanical properties[32]. This is connected to the material's internal stress and temperature, and under some circumstances, a shape memory effect takes place. When stress is placed between the Martensite and Austenite phases at a specific temperature, the austenite phase becomes distorted and retains its residual stress. This refers to this procedure as forward transformation. Here, distortion from the forward transformation is eliminated and the material reverts to its initial shape, a process known as reverse transformation, when heating is applied within the austenite phase, as shown in Fig. 1. SMA may be employed as an actuator during this process, which generates a significant amount of stress.

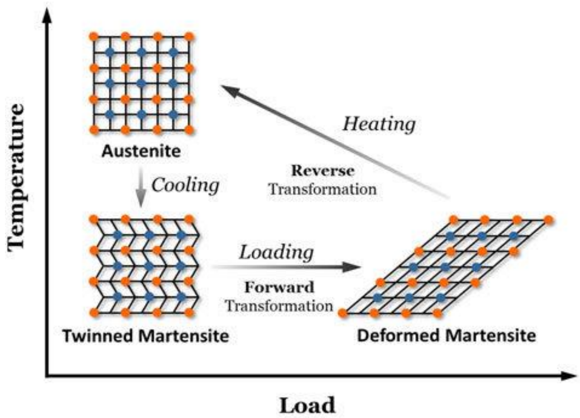

Fig. 1: Principles of working of SMA[33]

3. Modeling of SMA

The SMA demonstrates the exceptional ability to recall its prior crystalline configurations throughout the transition from the martensite to the austenite phase. In some applications, joule heating using electric current is the usual method of achieving actuation temperature. It is difficult to simulate the complex thermal-electrical-mechanical dynamics of SMA actuators. Additionally, the direct design and execution of the SMA model would provide challenges for the designers because of the fatigue behavior of SMA and its primary thermal mechanical conditioning. Even though the design, modeling, and dynamics of SMA actuators have been explored in a wide range of applications, there is relatively little research on systems based on SMA actuators in renewable energies, particularly about solar tracking and their control devices.

Micro and macroscopic levels were used by Khandelwal and Buravalla[34] to categorize SMA modeling approaches. The macroscopic research of SMA is more pertinent to actuator applications as it aims to understand phase field, hysteresis, and phase propagation. The SMA microscopic study deals with the dynamics of crystals and lattices. Three approaches may generally be used for the macroscopic investigation of SMA: 1) the thermodynamics model, 2) the phase transition model, and 3) the kinematic model.

In the proposed simulation for the SMA, the Thermodynamics model will be adopted.

3.1 Thermodynamic model of SMA

Temperature and current are two physical and electrical parameters related to the thermodynamics model of SMA. The difference between the power provided and heat losses determines the rate of temperature rise, as per the energy conservation rule[35,36]. The following is the thermodynamic equation:

$$\rho c \frac{\pi\, d_o^2\, L_o}{4}\frac{dT}{dt} = Ri^2 - \pi d_o L_0\, h(T - T_a) \qquad (1)$$

Where L_o = 1 m is the original length of the SMA spring, d_o = 0.5 mm is the diameter of the SMA spring wire. ρ = 6.45 g/m3 is wire material density, c = 837.36 J/kg.K is the specific heat coefficient, $R = 5\ \Omega$ is the wire electrical resistance, h = 47.83 is the coefficient of convective heat, $T(t)$ is the temperature, T_a = 20C° is the ambient temperature, $i(t)$ is the input current, and t is the time-independent variable.

It is possible to characterize the stress in the SMA spring as a function of temperature[32]:

$$Stress = Y(\alpha\Delta T)/L_o \qquad (2)$$

Where Y is young modules, α is the thermal expansion coefficient, and ΔT is the change of temperature.

A material experiences an increase in stress as displacement rises. This suggests that the more a material is stretched or twisted, the more stress it will experience. The relationship between displacement and stress is affected by the direction and magnitude of the applied force as well as the properties of the material, such as elasticity and stiffness.

At temperature T, the SMA spring actuator may provide the following output displacement[37]:

$$\delta(T) = \frac{[G(T) - G_L]\,\gamma_L}{(d/n\pi D^2)G(T) + [(F_H - F_L)/\Delta\delta F_L\,]G(T)\,\gamma_L} \qquad (3)$$

Where n is the spring's number of turns, F_L is the axial load at low temperature, F_H is the axial load at high temperature, d is the wire diameter, D is the average diameter of the spring, $\Delta\delta$ = 10 mm is the stroke of the actuator, γ_L = 2% is the shear strain, G_L is the shear modulus of the SMA spring at low-temperature value, and $G(T)$ is the shear modulus of the SMA spring at temperature T and its value (25–40) GPa in the austenitic phase.

At temperature T, the axial load may be found using[37]:

$$F(T) = \frac{\delta(T)G(T)}{\delta_L G_L}F_L \qquad (4)$$

The axial load at low temperatures can be given as[37]:

$$F_L = \frac{d^4 G_L}{8D^3 n}\delta_L \qquad (5)$$

4. System modeling

This study uses MATLAB R2023b Simulink to investigate the feasibility of employing SMAs as actuators to drive a single-axis solar tracker under open-loop control to drive a solar panel. The overall simulation model is displayed in Fig. 2. A simple smart actuator is built from two SMA springs; the first is used to drive the PV tracker at high temperatures and the second at low temperatures. Thus, to generate a displacement in response to heat input, SMA actuators exert a considerable force on a certain weight. The injected electric excitation current causes the suggested actuators to compress and have a substantial thermal energy storage capacity. It can then release this energy as displacement, or mechanical energy.

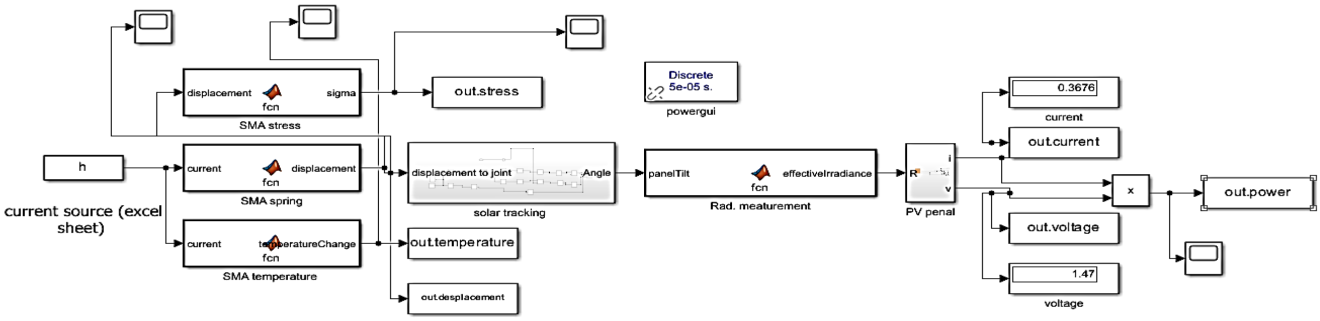

Fig. 2: Simulation of the entire solar tracking system model

To implement the tracker model, the first step is to build a framework. The framework used here is based on several stages. Firstly, an SMA model is built in which the displacement due to temperature change is obtained based on regulating the inlet excitation current values through a "current source Excel sheet" block. The displacement values exiting from the "SMA spring" block become input to the "solar tracking" block shown in Figure 3, built using a solid work program. The output of solar tracking block is the panel angle variable, which in turn becomes an input effective solar radiation from "Rad. measurement" block. The radiation value will become an input to the "PV panel" block. Lastly, the voltage and current values of the PV panel are recorded as the panel is loaded by a resistive load.

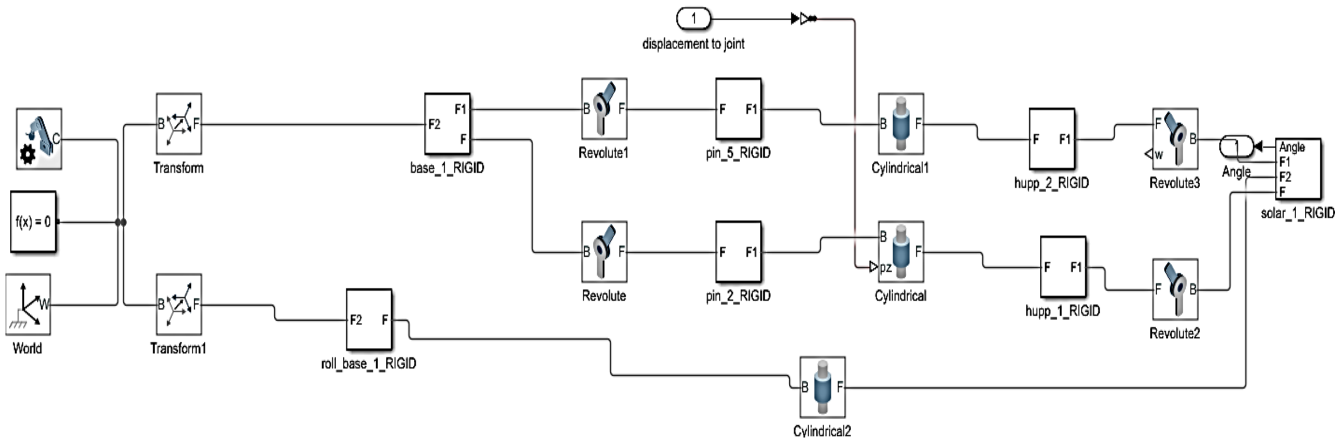

(a)

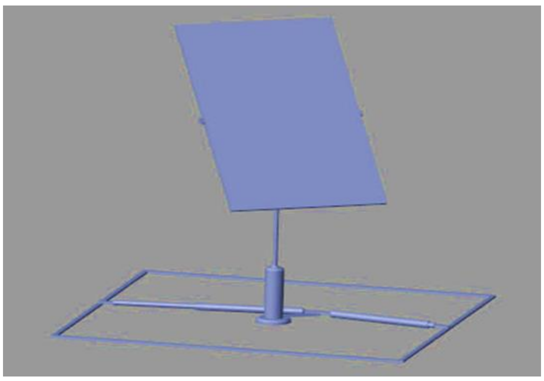

(b)

Fig. 3: a) Solar tracking block, b) solid work of PV panel block

Below is a detailed explanation of all subsystems (blocks) of the entire solar tracking system model shown in Fig. 2.

i. SMA spring block

The SMA spring block, shown in Figure 2 is used for modeling the two SMA springs based on the initial length, stiffness, and thermal properties of the SMA spring (thermal resistance, heat capacity, and ambient temperature). The input of this block is an Excel sheet of current and the output is the value of displacement of the SMA spring.

ii. SMA stress block

The SMA stress block is modeled to compute the SMA stress based on the spring parameters (spring constant and cross-section area of spring). The output of the SMA spring block, the "displacement", will be input to the SMA stress block and the output "sigma" of the SMA stress block acts as the stress of the SMA spring.

iii. SMA temperature block

The SMA temperature block is used to compute the SMA spring temperature based on the thermal characteristics of the spring. The Excel sheet of current will be fed to this block while, the output is the spring's temperature change.

iv. Solar tracking block

Solar tracking block is modeled to simulate the solar tracking mechanism. Its input is the displacement variable, which is the SMA spring's output and its output is the angle of the solar PV panel. All internal details of this block are shown in Figure 3a. The proposed solar tracking mechanism is built by attaching the SMA springs to the solar panel with a moving base. This base is connected to two cylinders on which the SMA spring will be placed. When the current passes through the SMA spring, the spring will cause a displacement. As a result of this displacement, the moving base will move and then the solar panel will rotate according to the displacement. The current feed values of the springs are related to the movement of the sun. They are stored offline in an Excel sheet to be called on time.

v. Rad. measurement block

The "Rad. measurement" block represents the relationship between the panel tilt angle as an input and the effective radiation as an output. The block is designed to evaluate the effective solar radiation incident on the PV panel based on the solar cell's tilt angle value. The output of this block, the effective irradiance, will be as an input to the "PV panel" block. The variations in radiation levels are taken from SunCal position on May 6, 2024, in Baghdad[31)].

vi. PV panel block

This block simulates the process of converting effective solar radiation falling on the solar panel into electrical power. The input to this block is effective solar radiation and the output is the electrical values represented by the voltage and current of the PV panel when loaded with a resistive load. The PV panel used has the specifications listed in Table 1.

Table 1. Solar panel specifications

Description	Value
Solar panel model	DG-P25W
Max. power (P_{max})	25W
Max. power voltage (V_{mp})	18V
Max. power current (I_{mp})	1.39A
Open–circuit voltage (V_{oc})	21.24V
Short–circuit current (I_{sc})	1.53A
Max. system voltage	1kV
Area of the solar cell	0.19 m^2

5. Experimental validation

An SMA-solar tracking system experimental setup under open-loop control is depicted in Fig. 4. The system mainly consists of a DG-P25W PV panel, a tracker's iron structure, control circuit, measuring sensors, Lead-Acid battery (2×12V, 9Ah), and two SMA springs. One end of each SMA spring is fixed at the point closest to the center of the PV panel to achieve rotation of the panel at the maximum possible angle. Since this spring has high strength characteristics, it has the ability to rotate the proposed plate up to 180° with minimal displacement. Each spring with an area of 19.65 mm^2 was formed from 1 mm diameter NiTi alloy wire. The control circuit mainly includes an Arduino UNO, ATS8W-43 Compact Analog Twin Timer to give signal each hour through the day to excite the spring with electric current pattern, and a general-purpose relay for turning on / off the SMA springs.

A series of experimental tests on displacement, temperature, and stress were carried out to assess the behavior of the SMA springs in response to changes in electric excitation current and to validate the simulation model's results.

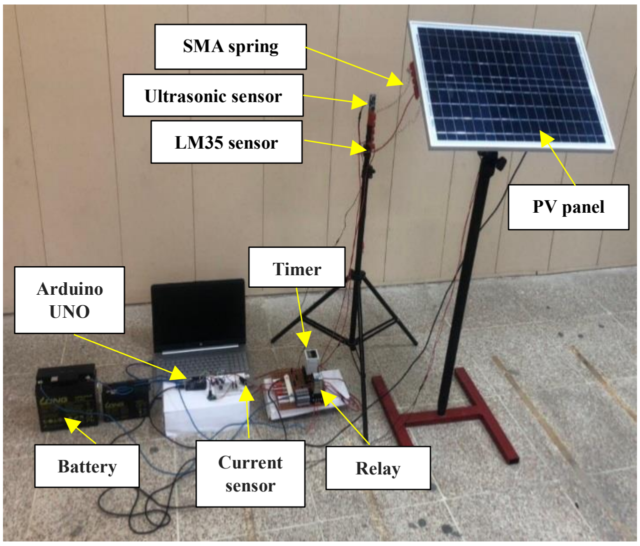

Fig. 4: Experimental setup

An Excel sheet table of electric current values is stored offline in the Arduino's RAM. The current values are proportional to the solar azimuth angles during the day of the test. These values are called sequentially according to the hours of the day in conjunction with the timer signal to excite the SMA actuators.

The necessary data values are captured by several sensors, such as a LM35 sensor to measure the temperature of the SMA spring, a load sensor to measure the force (i.e. stress = force/spring area) applied by spring to pull the PV panel, a ACS712 current sensor to measure the current flowing across the spring, and an Ultrasonic sensor HC-SR04 to measure the displacement in the spring.

The SMA springs will be activated by current table values shown in Fig. 5. All measurement (temperature, stress, and displacement) all based on electrically heated MSA springs. Figure 6-8 display the plotted current-dependent variables. By analyzing the results of Figs. 5-8, it is noted that there is a fairly acceptable agreement between the outputs of the simulation model and the experimental setup.

6. Results and discussion

This section describes the design and implementation of the SMA spring-driven solar tracking system model using MATLAB Simulink on May 6, 2024. The model results will also be validated by conducting experimental tests on the SMA-based solar system. The performance of the tracking system is studied in two stages. The first stage represented the study of SMA behavior during the day, while in the second stage, the behavior of SMA was reflected in the performance of the solar panel during the day in terms of their electric output power and efficiency.

6.1 SMA behavior

The hourly distribution of SMA spring excitation current is shown in Fig. 5. The values of current were determined according to the sun's azimuth angles in a full day and were stored off-line in a table (Excel sheet) to be entered into the SMA spring block. These currents were eventually converted within the model into a force that moves the solar panel at an angle proportional to the value of the current. The current table can be repeated during the days of the year based on maps related to the location of Baghdad city. In this case, the proposed system can work without the need for any feedback system, and this tracker can work in all expected weather conditions. Figure showed that the current increased from sunrise to sunset, with the exception of about midday, when it nearly stabilized because of the sun's slow movement and the high temperature during this time. This almost eliminated the need for electric current stimulation during this period. It can be seen from the figure that at the end of the day, the alloy draws the highest value of current to achieve the maximum displacement of the solar panel. The value of the excitation current in the practical side exceeds the theoretical one by approximately 16% throughout the day. This difference results from neglecting the loading effect to which the PV panel is exposed in the practical system, including air resistance and the coefficients of friction of the moving parts, etc.

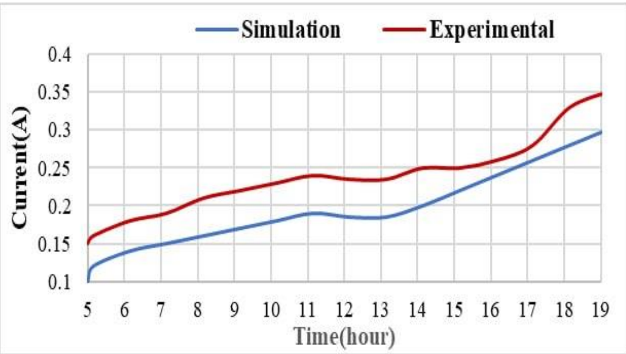

Fig. 5: Hourly distribution of SMA spring excitation current

The behavior of the SMA spring was studied in terms of changes in temperature, stress, and displacement during the day on May 6, 2024, as a function of excitation current, as shown in Figs. 6-8. Figure 6 shows how the temperature increased with increasing electric current (which was also the average temperature for the model), because increasing the current lead to increased energy loss and therefore an increase in the heat generated. It can be seen from the figure that at the end of the day, the practical temperature value of the alloy reaches approximately 70ºC. The practical values exceed the theoretical ones by about 10%.

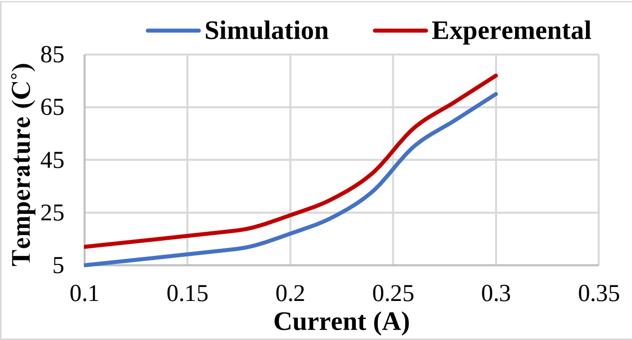

Fig. 6: Excitation current vs. temperature of SMA

The hourly change of the SMA stress with the SMA excitation current during the day is displayed in Fig. 7. Since the thermal expansion coefficient, which varied from alloy to alloy, was the primary factor determining stress, increasing the electric current resulted in increased heat production, which in turn raised the stress value. It was found that when electric current grew, so did the value of stress. In general, the more the temperature changes, the higher the level of stress that can occur. This increase lead to the transformation of the material into the austenite phase.

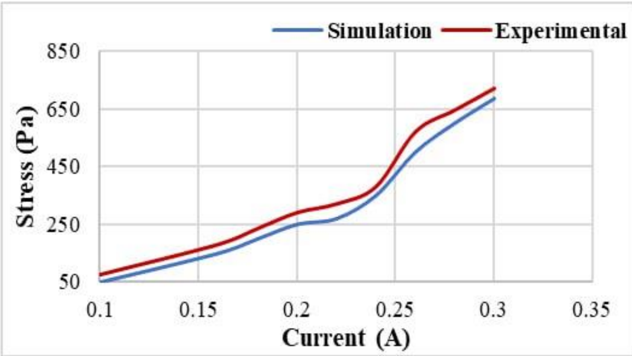

Fig. 7: Excitation current vs. stress of SMA

In addition, temperature-related modeling of the output displacement of the SMA spring actuator had been conducted. Figure 8 illustrates how the SMA spring actuator's output displacement rose in direct proportion to the excitation current. The opposing element defeats the readily bendable SMA element's resistance at low temperatures. To activate the actuator, the SMA element must be heated above the transformation temperature. Thus, the SMA element's stiffness increased, allowing it to overcome the contract's resistance and provide mechanical work and beneficial displacements. It can be seen from the figure that the spring displacement values were roughly steady for readings between 0.2 and 0.25 A, which correspond to noon. This is due to the sun's sluggish motion during that time of day.

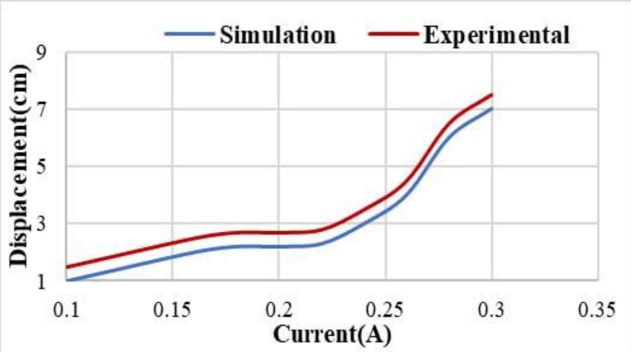

Fig. 8: Excitation current vs. total displacement of SMA

6.2 PV panel performance

Before beginning to study the performance of solar panels, the distribution of sun azimuth angles throughout the day must be known. The following data[38)] show additional information about timings: Dawn: 04:42:56, Sunrise: 05:09:24, Culmination: 11:59:20, Sunset: 18:49:45, Latitude: N 33°21'29.88"33.35830°, and Longitude: E 44°18'50.04"44.31390°. Coordinates: 38S 436167 3691219, considering that the solar declination = 16.7°. The sun azimuth angles were considered as the input signal to the PV block, whose movement reaches 216º, from east to west on May 6, 2024. The distribution of solar radiation during the day must be simulated. Figure 9 showed the distribution of solar radiation on May 6, 2024. It was noticed that the radiation gradually increased until it reached a maximum radiation of 1026 W/m^2 at noon and then began to decrease again.

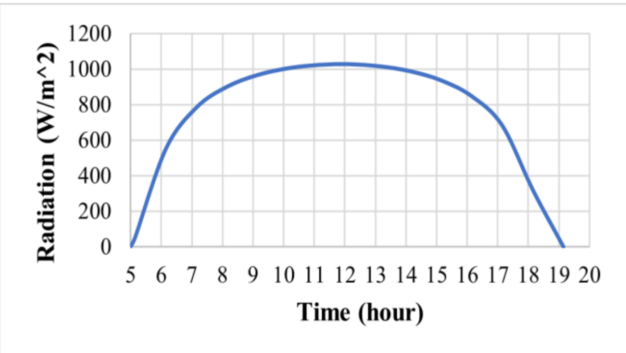

Fig. 9: Hourly distribution of solar radiation on May 6, 2024

The performance factors represented by the output power and efficiency of the PV panel were obtained and plotted, during the day on May 6, 2024, with and without tracking, as illustrated in Figs. 9 and 10.

The value of the PV panel's daytime electrical output power is shown in Fig. 10. It has been noted that the resultant energy rose until midday as the value of solar radiation climbed, and then it started to fall as the radiation value dropped. Additionally, at 12:30, the output power reached 20W without the tracking (fixed panel) and reached a maximum of around 25W while utilizing the tracker. It is noted that the maximum value of energy provided by the solar panel confirmed to the specifications of the PV panel in Table 1. The figure shows that the maximum performance of the mobile panel exceeds the fixed panel by 25%.

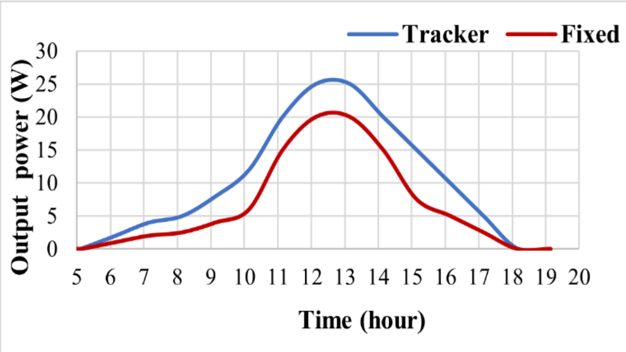

Fig. 10: Hourly distribution of PV panel output power

Plotting the PV panel efficiency curves was used the radiation intensity (G) curve (Fig. 9), the PV panel output curve (Fig. 10), and the panel area (A = 0.19 m^2). Eq. 7 offers a way to calculate efficiency.

$$\eta(\%) = \frac{P_o}{G \times A} \times 100\% \tag{7}$$

As illustrated in Fig. 11, the PV panel efficiency increased as solar radiation increased. The efficiency values began to gradually rise from sunrise at about 5:00 until they reached to maximum at midday around 12:30 and then began to decrease until they reached its lowest level at sunset around 18 o'clock due to the decrease in solar radiation. It was clear from the curves that the maximum efficiency reached about 13% in the case of tracking, while it is 10% without tracking. The maximum and average values of efficiency of the moving PV panel is greater than that of the fixed one by 30% and 60%, respectively.

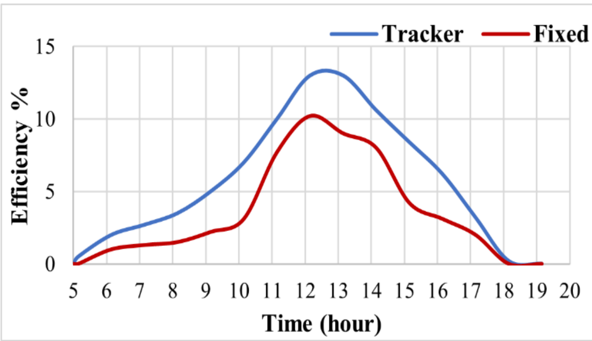

Fig. 11: Hourly distribution of PV panel efficiency

7. Conclusions

The study involved examining the system's performance and verifying the correctness of the computational model results through actual testing using a solar tracking system configuration based on SMA spring actuators. When compared to a fixed panel example, the moving panel's maximum efficiency increased by 30% at a solar radiation value of about 1026 W/m^2, demonstrating the importance of using smart technology to direct the tracking system. Additionally, it was discovered that, in comparison to a fixed panel, the panel powered by SMA actuators may raise its average efficiency value by 60% during the day. The outcomes proved that there is a lot of agreement between the experimental and analytical models. This alloy can be regarded as a good substitute for conventional actuators that power solar panels. The suggested system is incredibly low-cost and incredibly simple, and it can function offline without the requirement for feedback devices under all predicted weather conditions. Therefore, shadow or clouds have no effect on the movement and location of the tracker.

Acknowledgments

My sincere appreciation goes out to the to the Department of Biomedical Engineering (Electronics Lab) for their assistance, direction, support, in providing the necessary equipment to conduct the practical tests on the proposed tracking system.

References

1) P.A. Owusu, S.A.-Sarkodie, S. Dubey, "A review of renewable energy sources, sustainability issues and climate change mitigation", *Cogent Eng.*, 3 (1) (2016). https://doi.org/10.1080/23311916.2016.1167990
2) L.A. Rasheed, Mohammed, R.A. Jessam, "Performance Enhancement of a Single Pass Solar Air Heater by Adopting Wire Mesh Absorber Layer," *Evergreen*, 10 (2) 880-887 (2023). https://doi.org/10.5109/6792883
3) L.A. Rasheed, J.A.-K. Mohammed, R.A. Jessam, "Performance Enhancement of Solar Air Heater by Integrating Innovative Absorber Design and Automatic Control Flow Rate," *Evergreen*, 10 (3) 1439-1448 (2023). https://doi.org/10.5109/7151693
4) L.A. Rasheed, A.V. Yurchenko, V.I. Syryamkin, J.A.-K. Mohammed, "Optimization of Agricultural Drying using PCM Based Automated Indirect Solar Dryers," *Russian Physics Journal*, 66 (9) 983-989 (2023). https://doi.org/10.1007/s11182-023-03033-9
5) A.A. Ismaeel, H.A.A. Wahhab, Z.H. Naji, "Performance evaluation of updraft air tower power plant integrated with double skin solar air heater", *Evergreen* 8 (2) 296–303 (2021). https://doi.org/10.5109/4480706
6) R. Kumar, S.K. Verma, N.K. Gupta, S.K. Singh, "Performance Enhancement of TSAH using Graphene and Graphene/CeO2-Black Paint Coating on Absorber: A Comparative Study," *Evergreen* 9 (3) 673-681 (2022). https://doi.org/10.5109/4843098
7) Y.-D. Kim, K. Thu, K.C. Ng, Evaluation and parametric optimization of the thermal performance and cost effectiveness of active-indirect solar hot water plants, *Evergreen* 2 (2) 50-60 (2015). https://doi.org/10.5109/1544080
8) K. Tewari, R. Dev, "Analysis of modified solar water heating system made of transparent tubes & insulated metal absorber," *Evergreen* 5 (1) 62-72 (2018). https://doi.org/10.5109/1929731
9) O.A. Towoju, O.A. Oladele, "Electricity Generation from Hydro, Wind, Solar and the Environment", *Eng. and Tech. J.,* 39 (9) 1392-1398 (2021). https://doi.org/10.30684/etj.v39i9.2145
10) B. Belgasim, Y. Aldali, M.J.R. Abdunnabi, G. Hashem, K. Hossin, "The potential of concentrating solar power (CSP) for electricity generation in Libya," Renew. *Sustain. Energy Rev.* (90) 1-15 (2018). https://doi.org/10.1016/j.rser.2018.03.045
11) A. Musa, E. Alozie, S.A. Suleiman, et al., "A Photovoltaic Tracking Systems", *Information*, 14 (4) 211 (2023). https://doi.org/10.3390/info14040211
12) V.A. Kusuma, A.A. Firdaus, S.S. Suprapto, et al., "Comparative analysis of single-axis solar tracker performance with and without reflector under various weather conditions," *Int. J. Appl. Pow. Eng*. 13 (2) 328-334 (2024). https://doi.org/10.11591/ijape.v13.i2.pp328-334
13) V.S. Qader, O.M. Ali, N.I. Hasan, “An Experimental Comparison Between Fixed and Single-Axis Tracking Photovoltaic Solar Panel Performance: Zakho City as Case Study,” *Al-Rafid. Eng. J.*, 28 (1) 272–279 (2023). https://doi.org/10.33899/rengj.2022.136292.1204
14) F.M. Mohammed, J.A.-K. Mohammed, R.A. Nouri, "Efficiency Enhancement of a Dual-axis Solar PV Panel Tracker Using Water-Flow Double Glazing Technique," *Al-Khwarizmi Eng. J.* 14 (13) 32-47(2018). https://doi.org/10.22153/kej.2018.12.008
15) S.T. Hamidi, J.A.-K. Mohammed, L.M. Reda, "Design and Implementation of an Automatic Control for Two Axis Tracking System for Applications of Concentrated Solar Thermal Power," *Al-Khwarizmi Eng. J.* 14 (4) 54-63 (2018). https://doi.org/10.22153/kej.2018.01.010
16) H. Asyari, A.W. Aji, "Desain Solar Tracking Dual Axis Berbasis Arduino dan Sensor Light Dependent Resistor untuk Meningkatkan Daya Keluaran Sel Surya," *J. Tek. Elektro Uniba (JTE UNIBA)*, 7 (2) 320–324 (2023). https://doi.org/10.36277/jteuniba.v7i2.218
17) P. Muthukumar, S. Manikandan, R. Muniraj, T. Jarin, A. Sebi, “Energy efficient dual axis solar tracking

system using IOT," *Meas. Sens*. 28 (100825) (2023). https://doi.org/10.1016/j.measen.2023.100825

18) L. Halim, S. E. Gun, F. Wahab, "Solar Panel Efficiency Improvement through Dual-Axis Solar Tracking with Fuzzy Logic and Water Treatment Techniques," *J. Nas. Tek. Elektro*. 12 (3) 20–29 (2023). https://doi.org/10.25077/jnte.v12n3.1120.2023
19) L. Born, E.A.G.S. Martín, M. Ridder, et al., "FlectoSol – A pneumatically activable PV-functionalized façade shading module with bending motion in two directions for solar tracking," *Develop Built Envir.*, 18 (2024) ID: 100372. https://doi.org/10.1016/j.dibe.2024.100372
20) C. Alexandru, "Modelling and Simulation of a Hydraulically Operated Solar Tracker," *Renew. Energy and Power Quality J.*, 21 (1) 527-532 (2023). https://doi.org/10.24084/repqj21.383
21) H.M. Khalaf, J.A.-K. Mohammed, A.A. Altahir, "Simulation of Pneumatic Actuators under Fuzzy Logic Control for Driving Solar Tracking System," *Evergreen*, 11 (3) 1848-1855 (2024). https://doi.org/10.5109/7236836
22) M.A. Abdul-Hussein, J.A.-K. Mohammed, W.E. Abdul-Lateef, "Design of Pneumatic Actuators for Driving a Two-Axis PV Solar Tracker under Iraqi Climate Conditions", *Evergreen*, 11 (3) 1870-1881 (2024). https://doi.org/10.5109/7236838
23) E.S. Hassani, S.M. Saffar, Z.A. Ameer, "Preparation and Characterization of Biomedical Ni-Co-Al Shape Memory Alloys," *Eng. & Tech. J.*, 34 (7A) 1457-1472 (2016). https://doi.org/10.30684/etj.34.7A.17
24) M.K. Abbass, M.M. Kubaisy, R.S. Adnan, "The Effect of Thermo-Mechanical Treatment on Mechanical Properties & Microstructure for (Cu-Al-Ni) Shape Memory Alloy," *Eng. & Tech. J.*, 34 (13A) 2518-2526 (2016). https://doi.org/10.30684/etj.34.13A.14
25) E.S. Al-Hassani, A.H. Ali, S.T. Hatem "Investigation of Corrosion Behavior for Copper-Based Shape Memory Alloys in different Media," *Eng. & Tech. J.*, 35 (6A) 578-586 (2017). https://doi.org/10.30684/etj.35.6A.4
26) L. Sun, W.M. Huang, Z. Ding, Y. Zhao, C.C. Wang, H. Purnawali, C. Tang, "Stimulus-responsive shape memory materials: A review," *Mater. Des.* 33 (2012) 577-640. https://doi.org/10.1016/j.matdes.2011.04.065.
27) H. Baek, N.A., Mansour, A.M., Khan, V. Bijalwan, H.F.M. Ali, Y. Kim, "Correction to: SMA-based caterpillar robot using antagonistic actuation, "*Microsyst Technol.*, 29 (1223) (2023). https://doi.org/10.1007/s00542-023-05482-1
28) H. Du, G. Li, J. Sun, Y. Zhang, et al., "A review of shape memory alloy artificial muscles in bionic applications," *Smart Mater. Struct.*, 32 (10) (2023) 103001. https://doi.org/10.1088/1361-665X/acf1e8
29) M. Battaglia, A. Sellitto, A. Giamundo, M. Visone, A. Riccio, "Shape Memory Alloys Applied to Automotive Adaptive Aerodynamics," *Materials*, 16 (13) (2023) 4832. https://doi.org/10.3390/ma16134832
30) HG. Ozair. A.A. Khurram, A.U.H. Baluch, abdul Wadood, "Shape Memory Hybrid Composites for Aerospace Applications," *Mater. Scie. Forum*, 1068 (2022) 93-100. https://doi.org/10.4028/p-vd83mm
31) S. Kalra, B. Bhattacharya, B. Munjal, "Design of Shape Memory Alloy Actuated Intelligent Parabolic Antenna for Space Applications," *Smart Mater. & Struct.* 26(9) (2017). https://doi.org/10.1088/1361-665X/aa7468
32) C. Velmurugan, V. Senthilkumar, S. Dinesh, D. Arulkirubakaran, "Review on phase transformation behavior of NiTi shape memory alloys," *Mater. Today. Proc.*, 5 (6) 14597-14606 (2018). https://doi.org/10.1016/j.matpr.2018.03.051
33) W.S. Chu, K.T. Lee, S.H. Song, et al., "Review of biomimetic underwater robots using smart actuators," *Int. J. Precis. Eng. Manuf.*, 13 (2012) 1281–1292 https://doi.org/10.1007/s12541-012-0171-7
34) A. Khandelwal, V. Buravalla, "Models for shape memory alloy behaviour: an overview of modelling approaches," *Int J Struct Chang Solids-Mech Appl.*, 1(1) 111–148 (2009).
35) S.Q.-Guzman, S. Kannan, A.A.-González, et al., "Operational space control of a lightweight robotic arm actuated by shape memory alloy wires: a comparative study," *J. Int. Mater Syst Struct.*, 30 (9) (2017) https://doi.org/10.1177/1045389X17721050
36) N.T. Tai, K.K. Ahn, "Adaptive proportional-integral-derivative tuning sliding mode control for a shape memory alloy actuator," *Smart Mater Struct.*, (20) (5) (2011). https://doi.org/10.1177/1045389X17721050
37) J. Ma, H. Huang, J. Huang, "Characteristics Analysis and Testing of SMA Spring Actuator," *Adv. Mater. Sci. Eng.*, 2013, pp.7, Article ID 823594. http://dx.doi.org/10.1155/2013/823594
38) F.I. Mustafa, A.S. Al-Ammri, F.F. Ahmad, "Direct and indirect sensing two-axis solar tracking system," *in 2017 8th Int. Ren. En. Cong. (IREC), IEEE,* (2017). http://dx.doi.org/10.1109/IREC.2017.7926026

Appendix

ATI NiTi SMA 1™ Alloy

ATI

Technical Data Sheet

ATI NiTi SMA 1™ Alloy

INTRODUCTION

- Typically used in shape memory nickel titanium alloy devices and actuators
- Applicable industry standards: ASTM F2005, ASTM F2004, ASTM F2082
- Transformation temperature: Austenite finish (A_f) temperature range 30°C to 75°C
- (Determined in the fully solution annealed condition by DSC testing)

Table 1. Ingot Chemistry

Element	Typical maximum (unless noted otherwise) (weight %)
Nickel	54.0 to 57.0
Carbon	0.005
Cobalt	0.005
Copper	0.005
Chromium	0.005
Hydrogen	0.002
Iron	0.005
Niobium	0.005
Nitrogen + Oxygen	0.025
Titanium	Balance

Table 2. Physical Properties

Melting Point	1310°C (2390°F)
Density	6.45 g/cm^3 (0.234 lbs/in^3)
Electrical Resistivity	Austenite phase: ~80-100 μΩ-cm Martensite phase: ~70-80 μΩ-cm
Thermal Conductivity	Austenite phase: 0.18 watt/cm-°C Martensite phase: 0.085 watt/cm-°C
Thermal Expansion	Austenite: 11 x 10^{-6}/°C Martensite: ~6.6 x 10^{-6}/°C

Resource for additional physical properties:

- ASM Materials Properties Handbook: Titanium Alloys, ASM International Copy Right 1994

MECHANICAL PROPERTIES

Table 3. Mechanical Properties

Ultimate strength	>155 Ksi (1070 MPa)
Elongation	≥10%

(Yield strength and modulus depend on final product condition and testing conditions)

PRODUCT FORMS AVAILABLE

- Sheet: Nominal 0.020" to 0.125"T in widths up to 24" widths. Surface finish typically hot worked, blasted and pickled
- Plate: Nominal 0.126"T up to 0.250"T in widths up to 24" widths. Surface finish typically hot worked, blasted and pickled

Allegheny Technologies Incorporated
1000 Six PPG Place
Pittsburgh, PA 15222-5479 U.S.A.
www.ATImetals.com